International Journal of Pharmaceutics: X 7 (2024) 100234

Contents lists available at ScienceDirect

International Journal of Pharmaceutics: X

journal homepage: www.sciencedirect.com/journal/international-journal-of-pharmaceutics-x

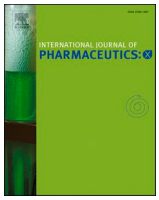

Design and validation of a custom-made system to measure transepithelial electrical impedance in human corneas preserved in active storage machine

Marielle Mentek [a,1], Benjamin Peyret [a,1], Siwar Zouari [a], Sébastien Urbaniak [a], Jean-Marie Papillon [a,b], Emmanuel Crouzet [a], Chantal Perrache [a], Sophie Hodin [c], Xavier Delavenne [c], Zhiguo He [a], Philippe Gain [a,d], Gilles Thuret [a,d,*]

[a] *Laboratory of Biology, Engineering and Imaging for Ophthalmology (BiiO), EA2521, Faculté de Médecine, Université de Jean Monnet, 10 rue de la Marandière, 42270 Saint-Etienne, France*
[b] *Papillon Engineering, Saint-Etienne, France*
[c] *INSERM U1059, Dysfonction Vasculaire et Hémostase, Université Jean Monnet, 10 rue de la Marandière, Campus Santé Innovations, Saint-Priest-en-Jarez, Saint-Etienne, France*
[d] *Département d'Ophtalmologie, Centre Hospitalier Universitaire, Avenue Albert Raimond, 42055 Saint-Etienne Cedex 02, France*

ARTICLE INFO

Keywords:
Corneal epithelial barrier
Corneal impedance
Corneal active storage machine
Benzalkonium chloride

ABSTRACT

Corneal epithelial barrier represents one of the major limitations to ocular drug delivery and can be explored non-invasively through the evaluation of its electrical properties. Human corneas stored in active storage machine (ASM) could represent an interesting physiological model to explore transcorneal drug penetration. We designed a new system adapted to human corneas preserved in ASM to explore corneal epithelial barrier function ex-vivo. A bipolar set-up including Ag/AgCl electrodes adaptors to fit the corneal ASM and a dedicated software was designed and tested on freshly excised porcine corneas ($n = 59$) and human corneas stored 14 days in ASM ($n = 6$). Porcine corneas presented significant and proportional decrease in corneal impedance in response to increasing-size epithelial ulcerations and acute exposure to benzalkonium chloride (BAC) 0.01 and 0.05%. Human corneas stored 14 days in ASM presented a significant increase in corneal impedance associated with the restoration of a multi-layer epithelium and an enhanced expression of tight junctions markers zonula occludens 1, claudin 1 and occludin. These results support the relevance of the developed approach to pursue the exploration and development of human corneas stored in ASM as a physiological pharmacological model.

1. Introduction

Cornea represents the first biological barrier protecting the ocular structures, in permanent contact with the environment. Corneal epithelium, composed of 5 to 7 layers of epithelial cells connected by three apico-lateral structures (tight and adherens junctions, and desmosomes), is the most superficial part of cornea and plays a major role in corneal barrier against biological, physical or chemical insults (Ban et al., 2003). By limiting the permeability of molecules across the cornea, it also represents one of the major barriers to ocular drug delivery through topical application (Leong and Tong, 2015). Topical application is an accessible and convenient method to deliver drugs at the ocular surface and to the anterior segment of the eye, thus it represents the preferred route of ocular drug delivery (Maulvi et al., 2021).

The study of transcorneal drug penetration and absorption can be conducted on a wide variety of models, from expensive in vivo approaches to simpler cell culture models (Agarwal and Rupenthal, 2016). Ex vivo models using isolated eyes or corneas from rabbit, porcine or bovine have been proposed as an affordable and more ethical alternative to in vivo experiments. However, the anatomical differences, limited accessibility and variable permeability results between species limit the use of these approaches, and most of these models are not accepted by regulatory bodies. Organotypic corneal equivalent or 3D corneal equivalents are promising economic and ethical alternatives allowing

Abbreviations: ASM, active storage machine; TEER, transepithelial electrical resistance; BAC, benzalkonium chloride; BSS, balanced salt solution; OC, organoculture; ZO-1, Zonula occludens-1; AUC, area under the curve; OD, oculus dexter; OS, oculus sinister.

* Corresponding author at: Ophthalmology Department, University Hospital, Saint-Étienne, France.
E-mail address: gilles.thuret@univ-st-etienne.fr (G. Thuret).

[1] The two first co-authors contributed equally to this work.

https://doi.org/10.1016/j.ijpx.2024.100234
Received 20 November 2023; Received in revised form 2 February 2024; Accepted 8 February 2024
Available online 9 February 2024

the reconstruction of human or animal corneal equivalent, including the 3 corneal cell types and an analogous structure (Kaluzhny and Klausner, 2021). However, these models are complex and still under development to reach standardization and acceptable accuracy.

The use of human corneal tissues is almost inexistent, as they are dedicated primarily to corneal transplantation, and would require the preservation of an intact and physiological corneal barrier after procurement. Despite a context of corneal tissue shortage for grafting (Gain et al., 2016), a substantial number of donor corneas are discarded by eye banks when the tissues are not suitable for grafting. The rate of non-conformity varies from 20 to 60% according to donors' selection criteria and eye-banks' medical and technical standards. Considering that 200 to 250,000 corneal grafts are performed yearly in the world (Gain et al., 2016), the number of human corneas discarded by eye banks is considerable. We recently described a new approach to preserve human corneas in close physiological conditions by restoring a transcorneal physiological pressure gradient similar to the intraocular pressure and by mimicking fluid circulation using an active storage machine (ASM) (Garcin et al., 2019). During storage of human corneas up to 3 months, this unique tool allowed us to improve corneal endothelial cell survival (Garcin et al., 2020) and their expression of Na+/K+ ATPase, regulate corneal stroma thickness and restore epithelial homeostasis (Guindolet et al., 2021). Morphological and ultra-structural exploration of human corneas stored in ASM, using immuno-histology and electron microscopy, confirmed the restoration of a mature and highly physiological corneal epithelium. Most interestingly, the infection of human corneas stored in ASM by herpes simplex virus 1 lead to the development of characteristic dendritic lesions and cytopathogenic effect highly comparable to the lesions developed by patients. These lesions were not described in existing ex-vivo models, and were directly related to the presence of a mature multilayer epithelium (Courrier et al., 2020). Taken together, these results support the pertinence of human corneas storage in ASM to develop alternative physiopathological models. Thus, human corneas stored in ASM represent an interesting surrogate and physiological model to explore transcorneal drug penetration and absorption. Such application would require a more comprehensive characterization of epithelium homeostasis and maturity in human corneas stored in ASM. However, the histological or biochemical techniques previously used to explore corneal epithelium in ASM are not suitable for a non-invasive exploration or follow-up of corneal barrier integrity during storage.

The evaluation of electrical properties of corneas in vivo (Guimerà et al., 2013; Uematsu et al., 2007, 2015) or ex vivo (Nakamura et al., 2010; Rojanasakul and Robinson, 1990) has been proposed as a non-destructive, sensitive and quantitative approach to explore corneal epithelial barrier function in whole corneas. This technique consists in passing an electric current through the tissue and measuring the voltage drop and potential difference across the tissue. Impedance (Z) is a two-dimensional vector value that consists of a real component, the resistance, and an imaginary component, the reactance. The most commonly used method for assessing impedance consists in measuring trans-epithelial electrical resistance (TEER), related to current flow dissipation, and whose main contributors are intercellular tight junctions (Srinivasan et al., 2015). Reactance, measures the opposition to the current produced by capacitive elements such as the phospholipid bilayer of the cell membranes, which acts as a capacitor due to its dielectric property (Ray et al., 2016). Thus, capacitance allows a direct measure of epithelial permeability linked to both paracellular pathway and cell membrane integrity (Wu et al., 2022). The resistance or the capacitance of the tissue is calculated using Ohm's law with the delivered current and the measured voltage (Macdonald et al., 2018).

The TEER is widely used for barrier integrity exploration using dedicated commercial systems in cellular models (Srinivasan et al., 2015). In particular, it allowed characterizing the effect of several drugs, ocular solutions or additives or to explore ion transport mechanisms in corneal cellular models (Fukuda and Sasaki, 2012; Ma et al., 2007).

Corneal electrical properties were studied on excised rabbit corneas (Donn et al., 1959; Nakamura et al., 2007; Rojanasakul and Robinson, 1990), but also on porcine (Juretić et al., 2018) and bovine corneas (Potts and Modrell, 1957). Fewer studies have explored corneal electrical in vivo in rabbits (Uematsu et al., 2015) and in humans (Biermann et al., 1991; Uematsu et al., 2016). The available data support the pertinence of corneal TEER measurements as a direct marker of epithelial barrier integrity. However, the comparison of the available data is very difficult as most of the published TEER values were measured at different frequencies and with very different equipment (electrode design and electrical set-up). It is accepted from other in vitro models that TEER measurements are poorly reproducible between laboratories and vary depending on the equipment used (Vandenhaute, 2011). The majority of available TEER data for ex vivo and in vivo corneas were obtained with custom-made systems and no commercially available device is adapted to our human corneal long-term storage system.

In the present work, we developed a complete system, adapted to human corneas stored in ASM, to measure impedance of whole corneas in nearly physiological conditions. To validate this new set-up, freshly excised porcine corneas were used as a model of intact corneal epithelial barrier and as models of physical and chemical injury. We then used our system on human corneas to measure the evolution of corneal electrical impedance as a direct marker of epithelial barrier integrity during storage in our ASM. Our goal is to validate a key tool to quantitatively monitor the corneal epithelial barrier in different storage conditions, in order to develop a reliable and pertinent corneal pharmacological model.

2. Material and methods

2.1. Impedance sensor and set-up

Corneal impedance was measured using a bipolar method, with 8 mm-diameter disc-shaped silver chloride electrodes (WPI, Saratose, FL, USA) placed on each side of corneas to allow uniform current density.

An electrical generator (33500B Serie Trueform, Agilent) connected in series with a 10 kΩ resistor (R), generated a 1 V alternative current. A multimeter (Fluke, 287 true RMS multimeter) placed in parallel with either the cornea alone to measure the voltage between the two electrodes (V_{out}), or placed at the terminals of the generator to control the effective voltage (V_{in}) (Fig. 1-A).

A custom-made software was programmed in C++ language (Qt creator) to automatically read and record the output voltages over a frequency range from 10 Hz to 1000 Hz. Each point was the average of 5 measurements repeated every 1500 ms. We performed 10 measurements points per decade (logarithmic scale): 10 points between 10 and 100 Hz and 10 points between 100 and 1000 Hz.

2.1.1. Electrode adaptation to corneal ASM

Electrode fixation was adapted to the design of the ASM, which allow maintaining human and porcine corneas in nearly physiologic conditions (Garcin et al., 2020; Guindolet et al., 2017).

Briefly the ASM was machined in biocompatible polyether ether ketone and maintain a sterile closed environment allowing long-term corneal storage. Under sterile conditions, the cornea is tightly secured to the ASM base, using the scleral rim as a watertight seal to separate the epithelial and endothelial chambers. The culture medium circulating in the chambers is continually renewed by a peristaltic pump associated with a pressure sensor, at a rate of 5 µl/min while creating a pressure in the endothelial chamber 20 mmHg higher than atmospheric pressure. As some ASM tubes are CO_2 permeable and the bicarbonate buffer enclosed in the culture media requires a 5% CO_2-enriched atmosphere, the ASM, except its control panel, was placed at 31 °C in a dry incubator with 5% CO_2.

Based on this set-up, a dedicated electrode holder was designed and

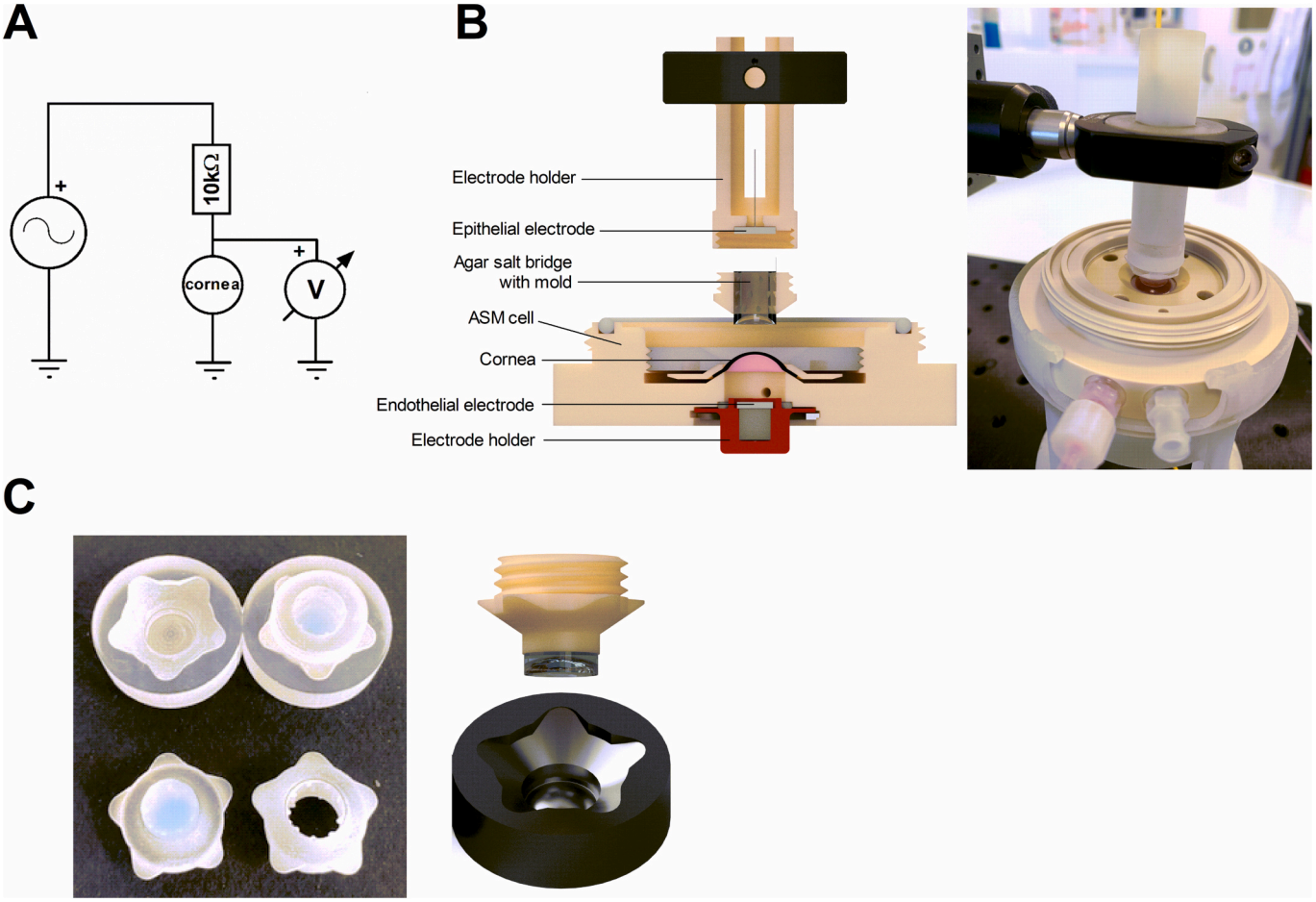

Fig. 1. Design of the system. A/ Schematic of the electrical circuit used to measure impedance of a cornea placed in the active storage machine (ASM) with a generator, a resistance of 10 kΩ and a digital voltmeter. B/ Cross section diagram and picture of the system showing the integration of one electrode in the endothelial chamber of the ASM cell owing to a dedicated holder, and the agar salt bridge with its mold screwed onto the epithelial electrode holder. C/ Picture and diagram of 3D-printed molds of the agar salt bridge and its 3D-printed holder. Spikes in the holder wall allowed good stability of the agar during experiments.

3D-printed in M2S-90HT polymer using Project MJP 2500 device (3D system, USA) to allow the placement of one electrode on the endothelial side of the cornea (Fig. 1-B, endothelial electrode). This electrode holder consisted of one portion designed to receive the electrode and to close hermetically the endothelial chamber (part A), and a second portion screwed into the first one to maintain the electrode and allow the passage of the electrode electric wire (part B). A silicone O-ring placed between the electrode and the electrode holder secured the sealing. The electrode area in contact with the storage medium was 0.502 cm^2.

To circumvent the leaking scleral tissue, the second electrode (epithelial electrode) was fitted to the corneal epithelial surface by using an agar salt bridge. Indeed, our preliminary results using a non-contact epithelial electrode (symmetrical to the endothelial electrode and in contact with preservation media) showed the absence of any corneal resistance, supporting a preferential passage of electrical current through the non-resistive scleral rim in contact with the preservation medium. Thus, electrical continuity was ensured by the preservation medium on the endothelial side, and by a salt bridge in agar in contact with the epithelial side.

Agar salt bridge, composed of 3% agar agar (Euromedex, Souffelweyersheim, France) in balanced salt solution (BSS, Alcon, USA), was molded to fit corneal curvature using custom-made molds (Fig. 1-C). The concave side of the agar gel adhered completely to the corneal surface, and the opposite flat side was is in contact with the second measuring electrode. The diameter of the agar gel was standardized to 8 mm. The mold was designed to be directly screwed onto a dedicated electrode holder, allowing perfect contact between the agar salt bridge and the electrode. The ASM cell was immobilized while the electrode holder was mobilized on the z axis using a micrometric screw for repeatable positioning of the agar salt bridge on the corneal surface. Temperature was recorded during experiments using a thermometer probe placed in the electrode holder.

2.1.2. *Impedance calculation*

The measured V_{out} (in mV) was the voltage (electric potential difference) across the two electrodes through the cornea. V_{in}, the effective voltage equivalent to the root mean square of the delivered tension, was measured at 353.55 mV and was checked prior to each impedance measurement. The impedance Z (characteristic of alternating current) was calculated using the following formula:

$$Z = Vout^{*} R/(Vin - Vout)$$

For each cornea, impedance was measured in the presence and in the absence of the cornea, the latter condition reflecting the resistance of electrodes and storage media. The value of impedance between the electrodes without the cornea was substracted to the impedance values measured with the cornea. The values of impedance were normalized to the surface of the electrodes (0.502 cm^2) and expressed in Ohms.cm^2.

2.1.3. *Electrical modeling of porcine cornea*

As corneal impedance in function of current frequency was highly similar to a low-pass filter signal (Obeid et al., 2017), the electrical

modeling of cornea was obtained through fitting a passive second order low-pass model to corneal impedance results by iteration (Zhang and Zhu, 2010). The obtained corneal impedance results were compared to electrical models using the simulation software Tina-Ti (Texas Instrument, USA). Coefficients values were then calculated from the most relevant model by least squares method using the following formula:

$$R = \sqrt{\frac{\sum_i \left(y_i^{exp} - y_i^{cal}\right)^2}{\sum_i y_i^{exp2}}}$$

The model was tested on all tested porcine corneas (baseline measures in intact corneas, $n = 59$) to evaluate inter-corneal variability of the coefficients of the model. The coefficients were also calculated for corneas with mechanical and chemical damage (see below).

2.2. Experimental procedures

2.2.1. Human and porcine corneas

To validate the impedance measurement set-up and technique, we first worked with freshly excised porcine corneas mounted in the ASM, as a pertinent and well described model of intact corneal epithelial barrier. After validation, we aimed to measure impedance of human corneas after different duration and condition of storage, as the final application of the approach to explore corneal epithelial barrier. Comparison of impedance values between the two different samples was not the goal of the experiments.

Porcine corneas were procured from a local slaughterhouse immediately after animal death (before scalding) and were used for experiments within 6 h after procurement. Ocular globes were stored in balanced salt solution (BSS) at 4 °C until use. Fifty-nine porcine corneas were used for impedance measurements.

Human corneas unsuitable for transplantation were obtained from the eye banks of Saint-Étienne and Besançon after informed consent of the relatives, as authorized by French bioethics laws. Handling of donor tissues conformed to the tenets of the Declaration of Helsinki for biomedical research involving human subjects. Corneas were deemed unsuitable for transplantation because of a low endothelial cell count (<2000 cells/mm^2) or non-conclusive serology tests. Six corneas from 3 donors (1 man and 2 women) with a mean age of 74 ± 6 years were used. Corneas were procured at a mean time of 7.5 ± 5 h after death. Corneas were stored at 31 °C in sealed glass flasks of standard organ culture (OC) medium (Corneamax; Eurobio, Les Ulis, France) in a dry incubator, without medium renewal, during 7 weeks, 3 weeks and 1 week (corneal pair 1, 2 and 3 respectively). These parameters represent standard organoculture (OC) conditions. Additionally, 2 corneas (not paired) from 2 donors (1 man [70 years], 1 woman [81 years]) were used for assessing corneal epithelial barrier after 3 weeks of OC (histology and immunostaining).

2.2.2. Assessment of porcine corneal epithelium prior to impedance measurements

Porcine corneas were excised from the eyeball but cutting the sclera 5-mm from the limbus and immediately secured in the ASM base as previously described (Guindolet et al., 2017). The endothelial chamber was then filled with CorneaMax and pressure maintained at 21 mmHg in the endothelial chamber. Superficial epithelium quality was assessed by fluorescein staining. After applying one drop of fluorescein Faure 0.5% (Théa, France) followed by rinsing with BSS, the cornea was imaged using a macroscope (Olympus MVX50) under FITC channel (488 nm). Absence of fluorescent staining was the criteria to use the cornea in impedance measurements. Corneas presenting focal or generalized fluorescent labeling were discarded (Fig. S1).

2.2.3. Corneal impedance variation in response to epithelial ulceration

Measurements were performed first on intact corneas and were used as baseline values. Impedance was then measured after performing ulcers of increasing size: 1 mm, 2.4 mm and 4 mm using corneal trephine and a crescent knife. Finally, a last measurement was performed after complete removal of the remaining corneal epithelium ($n = 18$ corneas). The same measurement protocol was performed in control corneas ($n = 6$) for which the epithelium was kept intact. For each condition, five measurements (repeated every minute) were performed and averaged. The cornea and agar were hydrated with BSS between the repeated measurements. At the end of the experiment, to evaluate epithelial integrity after repeated measurements, the control corneas were fixed in 4% PFA and further processed for hematoxylin-eosin-saffron staining on paraffin sections.

2.2.4. Corneal impedance variation in response to exposure to benzalkonium chloride (BAC)

The acute effect of BAC on corneal impedance was assessed in 35 porcine corneas.

For each pair of corneas, one cornea was exposed to BAC 0.05% or 0.01% (Thermo Fisher Scientific; dissolved in BSS) whereas the second cornea was used as control (BSS). After measurements on the intact cornea, the corneal surface was incubated during 2 min with either BAC 0.05% or 0.01% or BSS, then rinsed with BSS. The impedance was measured again after the incubation period. For each condition, five measurements (repeated every minute) were performed and averaged.

2.2.5. Corneal impedance of human corneas stored in active storage machine

Impedance was assessed in 3 pairs of human corneas before (D0) and after 14 days of storage in ASM (D14). At D0, impedance measurements were performed as described above, in sterile conditions. Corneas were then stored in ASM during 14 days as previously described (Garcin et al., 2019; Guindolet et al., 2021). A pressure of 20 mmHg was maintained on the endothelial side while the storage medium was renewed at a rate of 2.6 µl/min. The corneas in ASM were placed at 31 °C in a dry incubator with 5% CO_2. Corneal thickness was assessed at D0 and D14 by OCT (Casia I, Tomey, Nagoya, Japan). Epithelium macroscopic morphology was followed at D0, D7 and D14 by OCT (ATR 206 with OCT-LK4-BB lens kit, Thorlabs, Newton, NJ, USA) and by macroscopy (macro-zoom microscope, MVX10, Olympus). At the end of D14 measurements, 1/4 of each cornea was fixed in 4% PFA and further processed for hematoxylin eosin saffron staining on paraffin sections. The remaining 3/4 was fixed in 0.5% PFA during 45 min to explore expression and distribution of tight-junction proteins by immunohistochemistry on flat-mounted cornea, following the same protocol described above for porcine corneas.

2.2.6. Exploration of epithelial barrier integrity after impedance measurements

The expression and distribution of tight junction proteins was explored by immunohistochemistry on flat-mounted tissues after impedance measurements in porcine corneas treated with or without BAC ($n = 3$ per condition), on human corneas at Day 14 and on the 2 human corneas stored for 3 weeks in OC. At the end of the experiment or storage period, corneas were fixed in 0.5% PFA during 45 min. After fixation, corneas were permeabilized in 0.1% Triton (Sigma) for 10 min at room temperature, then rinsed three 5 min-times in phosphate-buffered saline (PBS). Nonspecific binding sites were blocked by incubation for 30 min at 37 °C in PBS supplemented with 2% heat-inactivated goat serum (Eurobio) and 2% bovine serum albumin (Thermo Fisher Scientific). Corneas were then incubated overnight at 4 °C with primary antibody against E-cadherin (mouse; BD Pharmigen, 562,869), zonula occludens-1 (ZO-1; rabbit; Invitrogen, 40–2200), claudin 1 (Santa Cruz Biotechnology, sc-16,639) or occludin (Santa Cruz Biotechnology, sc-133,256) diluted at 1:200. After three 5 min-rinsing in PBS, samples were incubated for 1 h with Alexa Fluor 488 goat anti-mouse and Alexa Fluor 555 goat anti-rabbit IgG (Invitrogen, Eugene, USA), 1:500 diluted in blocking buffer. Filamentous actin was labeled at

this step using iFluor 555-conjugated phalloidin diluted 1:500 (phalloidin-iFluor 555, Euromedex, France) whereas nuclei were counterstained for 10 min with 40,6-diamidino-2-phenylindole dihydrochloride (5 µg/ml in PBS). Corneas were finally flat-mounted using Vectashield medium (Vector Laboratories, Burlingame, USA). Images were captured with a confocal microscope (IX83 Fluoview FV-1000; Olympus), equipped with the Olympus Fluoview software. The image acquisition parameters (laser power, 13%) were identical for all corneas.

2.3. Statistical analysis

Statistical analyses were performed with GraphPad Prism 5 software (GraphPad Software, San Diego, CA, USA). Area under the curve (AUC) was calculated for each measure between 10 and 1000 Hz and used as representative impedance value for each tested experimental condition. Data, assessed by Shapiro-Wilk test, were not normally distributed, thus experimental groups were compared using non parametric tests. The AUC values from distinct conditions were compared using Kruskal Wallis test whereas impedance curves from 10 to 1000 Hz were compared using Friedman one-way repeated measure analysis of variance, both followed by Dunn's Post-hoc analysis. Data are represented as median and interquartile range. $p < 0.05$ was considered significant.

3. Results and discussion

3.1. Variable impedance measured in intact porcine corneas

Corneal impedance of intact porcine corneas varies greatly between samples in the studied frequency range (Fig. 2-A). Coefficient of variation, calculated for each frequency, ranges from 40 % (1000 Hz) to 55% (12.6 Hz), indicating a high variability among the explored corneas ($n = 59$). When analyzing the distribution of tested corneas among the impedance AUC range, the great majority impedance AUC were comprised between 5.0×10^5 and 1.5×10^6 (Fig. 2-B). As shown in Table 1, it is very difficult to compare the available data about corneal

Table 1
Corneal impedance measurements at different frequencies (from the literature and our results).

Author, date	Species (model)	TEER (frequency)	TEEI (frequency) in our study (Porcine, ex vivo)
Nakamura, 2010	Rabbit (ex vivo)	≈ 1000 Ω.cm^2 (0.017 Hz)	NE
Juretic, 2018	Porcine (ex vivo)	604 to 829 Ω.cm^2 (2 Hz)	NE
Uematsu, 2016	Rabbit (in vivo)	750 ± 111 Ω.cm^2 (12.5 Hz)	
Uematsu, 2007	Rabbit (in vivo)	602.3 ± 195.0 Ω.cm^2 (12.5 Hz)	891 ± 346 Ω.cm^2 (12.6 Hz)
Chen, 2012	Rabbit (in vivo)	832.1 ± 107.3 Ω.cm^2 (12.5 Hz)	
Kusano, 2010	Rabbit (in vivo)	741.4 ± 228.4 Ω.cm^2 (12.5 Hz)	
Rojanasakul, 1990b	Bovine (ex vivo)	800 Ω.cm^2 (500 Hz)	706 ± 232 Ω.cm^2 (501.2 Hz)

NE, not evaluated. TEER, transepithelial electrical resistance; TEEI, transepithelial electrical impedance.

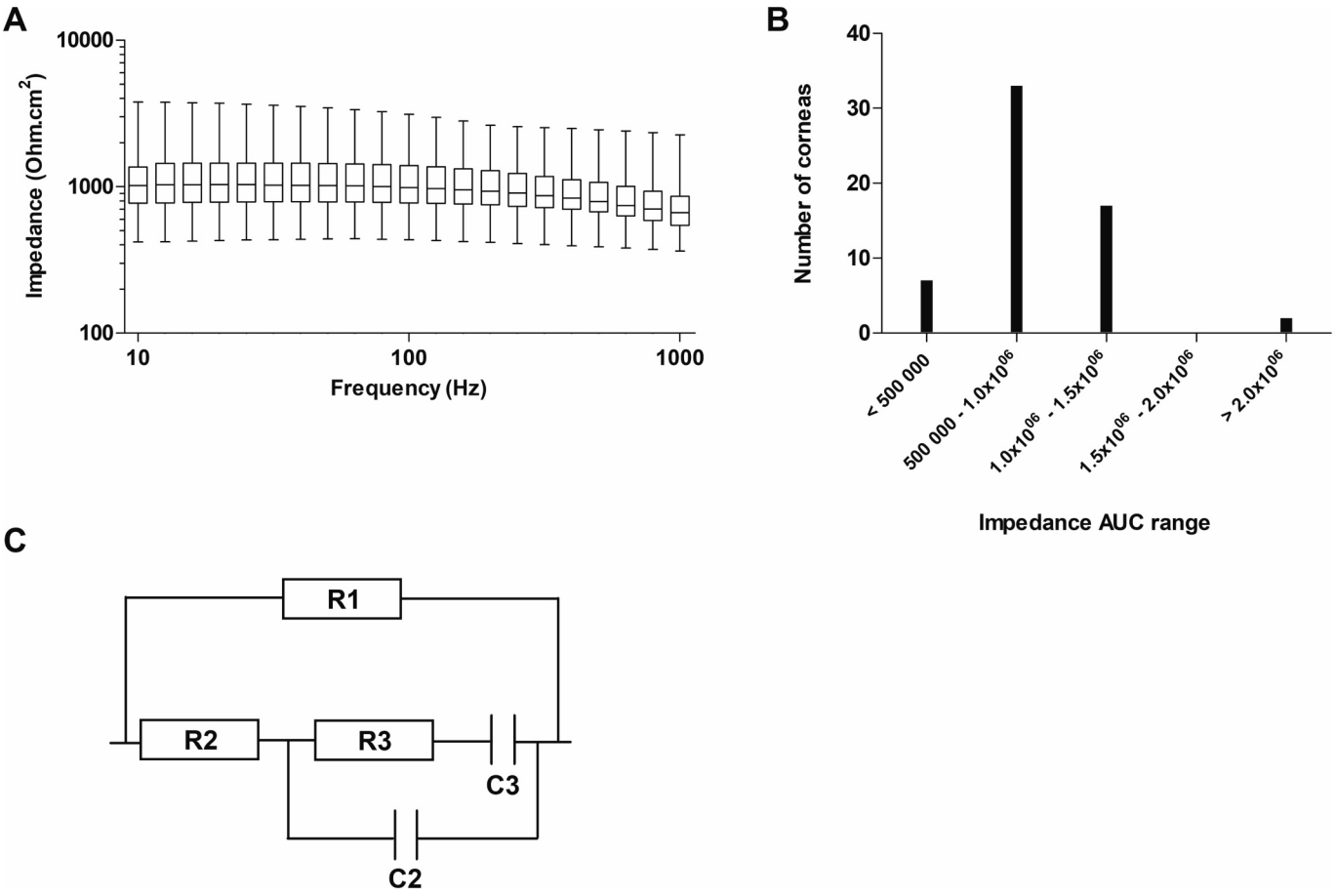

Fig. 2. Corneal impedance measured in intact porcine corneas (n = 59). A/ Box-plot representing corneal impedance (in Ω.cm^2) over the studied frequency range (10 to 1000 Hz). Data are provided as median, interquartile range with minimum and maximum values. B/ Distribution of corneal samples in function of impedance AUC value calculated between 10 and 1000 Hz. C/ Equivalent circuit of fresh porcine corneas.

impedance upon the studies considering the variable species and models described, but also the electrical parameters and electrode design used. Among the reported variable parameters, the current frequency at which the impedance is recorded vary markedly among studies, from extremely low to low frequencies below 20 Hz (Juretić et al., 2018; Rojanasakul et al., 1990; Uematsu et al., 2007) to very high frequencies, up to 10 kHz (Guimera et al., 2012; Jürgens et al., 1996). An alternative current square wave with a frequency of 12.5 Hz, from a widely used ~~a~~ commercial setup, was designed to avoid charging the cell layer and the electrodes and for cell culture application. These electrical parameters were also used to explore corneal resistance in vivo in rabbit (Uematsu et al., 2007) and in humans (Uematsu et al., 2016).

The dielectric properties of a biological system are frequency dependent. It has been shown that the 1 kHz to 10 MHz frequency range allows exploring the polarization of cellular cytoplasmic membranes, acting as barriers to the ions flow between the intra- and extra-cellular media (Gabriel, 1995; Schwan, 1957). It is thus accepted that tissue-related resistance and capacitance are contributing predominantly to the total impedance signal measured within this frequency range (Benson et al., 2013).

Usually, the reported working frequencies in cellular or corneal models are below this range. Guimera et al. previously showed that the corneal epithelium has the largest contribution in corneal impedance in frequency under 50 kHz (Guimera et al., 2012). Using our setup, the impedance values of intact corneas on frequencies over 1 kHz were comparable to storage media alone values. Previous measurement of corneal impedance in the range from 10 kHz to 10 MHz showed that cornea was comparable to saline solution (Jürgens et al., 1996). Indeed, at high frequencies the capacitors of cellular membranes become more conductive and the total impedance of the studied biological barrier

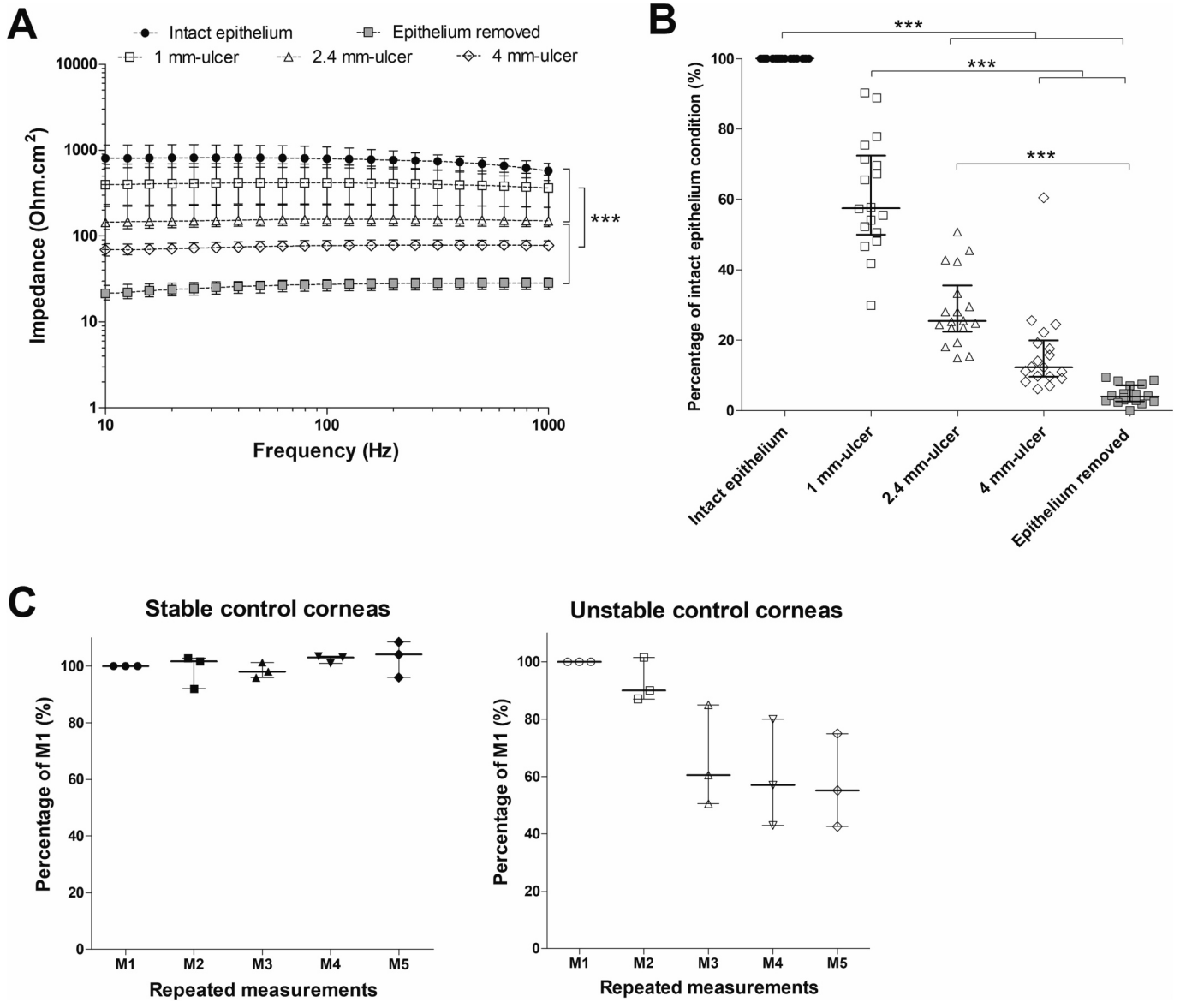

Fig. 3. Evolution of corneal impedance in response to epithelial ulceration. Increasing area of epithelial ulceration of 1 mm, 2.4 mm, 4 mm diameter and complete removal of the corneal epithelium ($n = 18$ corneas) were tested. A/ Raw impedance in $\Omega.cm^2$ from 10 to 1000 Hz for each condition (median with interquartile range) . ***$p < 0.0001$, Friedman test with Dunn's post-hoc analysis. B/ Impedance AUC values expressed as percentage of the baseline value (intact epithelium condition). ***$p < 0.0001$, Kruskal Wallis test. Statistical significance is displayed only for the closest groups in the two graphs. C/ Impedance AUC values expressed as percentage of the baseline value (first measure [M1] with intact epithelium) for the control corneas. Analysis of the signal variation with time (repeated measures M1 to M5 with intact epithelium) showed two tendencies, with corneas presenting a stable signal over repeated measurements ($n = 3$, right-hand graph) and corneas showing an unstable signal with progressive and moderate decrease of impedance signal over time (n = 3, left-hand graph).

converges to the resistance of the medium. As there is no clear data to support the exploration of biological barrier at a preferential single frequency, we choose to use the impedance data over a frequency range rather than at an isolated frequency. This frequency range includes most of the frequencies previously described for corneal impedance exploration and allowed us to discriminate well described corneal epithelial barrier alteration.

The influence of experimental parameters on baseline impedance was explored. Indeed, the variable time between eyeball procurement and corneal impedance measurement (1.5 to 6 h) could cause variable epithelial barrier damages and thus be involved in the observed variability in baseline corneal impedance. When comparing impedance AUC values in function of the order of processing over experimental sessions (Fig. S2-A and B), there was no significant difference between samples according to time between procurement and measurement. Similarly, the variability in corneal epithelial quality after procurement over the different experimental sessions (days) could be implied in this variability. However, there was no significant differences between the impedance AUC values measured during the different experimental sessions (Fig. S2—C and D). The most reported limitations of corneal impedance ex vivo assessment are: 1/ corneal damage while preparing for the experiment, 2/ the variation of corneal hydration by the buffer solution during the experiment, 3/ the instability of measurement at the beginning of the experiment. In our case, potential corneal damages are very limited as the cornea is secured on the chamber behind the limbus. Only epithelial alteration during procurement and transport may impact the state of corneal barrier and thus impedance values. This last aspect contributes most probably to the variability of impedance results between samples in our experiment, frequently reported by other teams (Uematsu et al., 2007, 2016).

3.2. Decrease of corneal impedance in response to a mechanical stress

The evolution of corneal impedance in response to increasing area of epithelial ulceration is shown in Fig. 3.

Corneal impedance decreased significantly and proportionally to the increasing area of epithelial ulceration ($n = 18$, $p < 0.0001$, Friedman test with Dunn's post-hoc analysis, Fig. 3-A). Impedance AUC decreased by 42.5 (9.8 [min] - 70.2 [max]), 74.6 (49.2–85) and 87.7% (39.5–93.8) in response to 1 mm, 2.4 mm and 4 mm-ulceration respectively. After corneal epithelium complete removal, impedance AUC was 4.0% (0.1–9.4) of the baseline impedance value (Fig. 3-B). Each experimental condition was statistically different with the others, excepted for the closest ulceration condition (Table S1). To our knowledge, it is the first time that the discriminative capacity of impedance measurement related to the area of altered corneal epithelium is explored. Complete or partial mechanical abrasion of corneal epithelium is a simple and invasive way used to explore the permeability and the electrical resistance of the different corneal components (Potts and Modrell, 1957; Prausnitz and Noonan, 1998). We choose to perform increasing-size ulcerations as a model of corneal re-epithelialization process, in order to explore the capacity of our system to discriminate close-size ulcers by measuring corneal impedance. The final goal would be to be able to quantify epithelial renewal process in human corneas during storage in ASM or during epithelial healing after iatrogenic ulceration. Our results support a discrimination of ulcers of size differing from >2 mm diameter, which could reveal sufficient in the two previous applications. However, the current system cannot discriminate more subtle variation of epithelial surface. Additional experiments on re-epithelizing human corneas should be performed to explore this aspect.

In control corneas, subjected to repeated measurements over the same experimental duration without alteration of corneal epithelium, impedance signal showed two trends in behavior (Fig. 3-C). Impedance was stable over time for half of the control corneas whereas the remaining half corneas presented a continuous decrease of impedance signal over time. Taken together, the impedance signal in all control corneas did not significantly vary over time ($n = 6$, $p > 0.05$, Kruskal Wallis test). These results highlight the limitation of variable time-related degradation of biological barrier when using fresh tissues in pharmacological studies.

The corneal epithelium presented comparable mature and physiological pluristratified structure (6 to 7 cell layers) in histologic sections of both freshly procured corneas and corneas after impedance measurements, independently of the experiment (Fig. 4-A).

3.3. Decrease of corneal impedance in response to a chemical stress

In comparison to baseline impedance values and control group, the incubation of corneal surface with 0.01% and 0.05% BAC triggered a significant decrease in corneal impedance ($n = 9$ per BAC group, $p < 0.001$, Friedman test with Dunn's post-hoc analysis) (Fig. 5-A and B).

Corneal impedance AUC decreased by 25.4 (12.6–36.9) and 63.8% (44.5–68.3) in response to 0.01% and 0.05% BAC respectively (Fig. 5-C). Control corneas did not present any significant variation of impedance after incubation with BSS.

Immunostaining on flat-mounted porcine corneas showed a degradation of the expression of tight-junctions proteins after incubation with BAC (Fig. 4-B). In control group, ZO-1, claudin 1 and occludin labelling presented a uniform and continuous expression at the cell membrane (cell-cell boundaries) of the most superficial corneal epithelial cells. Immunostaining signal observed after BAC 0.01 and 0.05% was spatially more heterogenous and fragmented. Benzalkonium chloride is the most widely used preservative in ocular formulations, with antimicrobial and surfactant properties. Despite initial good ocular tolerance observations, increasing studies agreed on a long-term detrimental effect for ocular surface health (Vaede et al., 2010).In a rabbit model, BAC has be shown to promote in vivo corneal epithelial barrier leakage, through tight-junctions disruption between epithelial superficial cells, associated to a concentration-dependent decrease in corneal impedance (Chen et al., 2012). Accordingly, BAC is widely used to efficiently increase the paracellular permeability of corneal epithelium, monitored by corneal impedance transepithelial resistance measurement (Chetoni et al., 2003; Guimerà et al., 2013; Kusano et al., 2010; Uematsu et al., 2007). Concentrations of BAC as low as 0.0001% were able to significantly alter corneal impedance (Chetoni et al., 2003), whereas the maximal reported concentration (0.2%) provoked a decrease of 91.8% of corneal impedance (Guimerà et al., 2013). The decrease in corneal impedance promoted by BAC ranged from 30 to 70% for BAC 0.01% (Guimerà et al., 2013; Kusano et al., 2010) and from 77 to 80% for BAC 0.05% (Guimerà et al., 2013; Uematsu et al., 2007). In a rabbit model of chronic ocular instillation of BAC, corneal barrier leakage was confirmed by a BAC dose-dependent increase in corneal permeability to carboxy fluorescein, and associated with similar alterations in ZO-1 localization (Chen et al., 2011). The alteration in tight-junction proteins seems more pronounced after BAC 0.05% in comparison to BAC 0.01%. Our results, showing BAC concentration-dependent decrease in corneal impedance associated with alteration in tight junction proteins expression, are in accordance with previous reports and support again the relevance of impedance measurement to non-invasively explore alterations of the corneal epithelial barrier.

3.4. Exploration of equivalent electrical model of the porcine cornea

The equivalent circuit of fresh porcine corneas obtained in our model is showed in Fig. 2-C and was characterized by two cascade RC cells (R2, C2 and R3,C3) in parallel with a third resistance R1, all contributing to the impedance signal measured in these experiments. The resistances R1 and R3 were the major contributor to corneal resistance with median values of 1012 Ω (431–3573 [min – max]) and 1624 Ω (497–4206) respectively. Capacitors C2 and C3 were associated with low capacitance values of 9.10^{-8} and 8.10^{-8} F (median value) respectively. This model is in accordance with the corneal equivalent circuit describe by

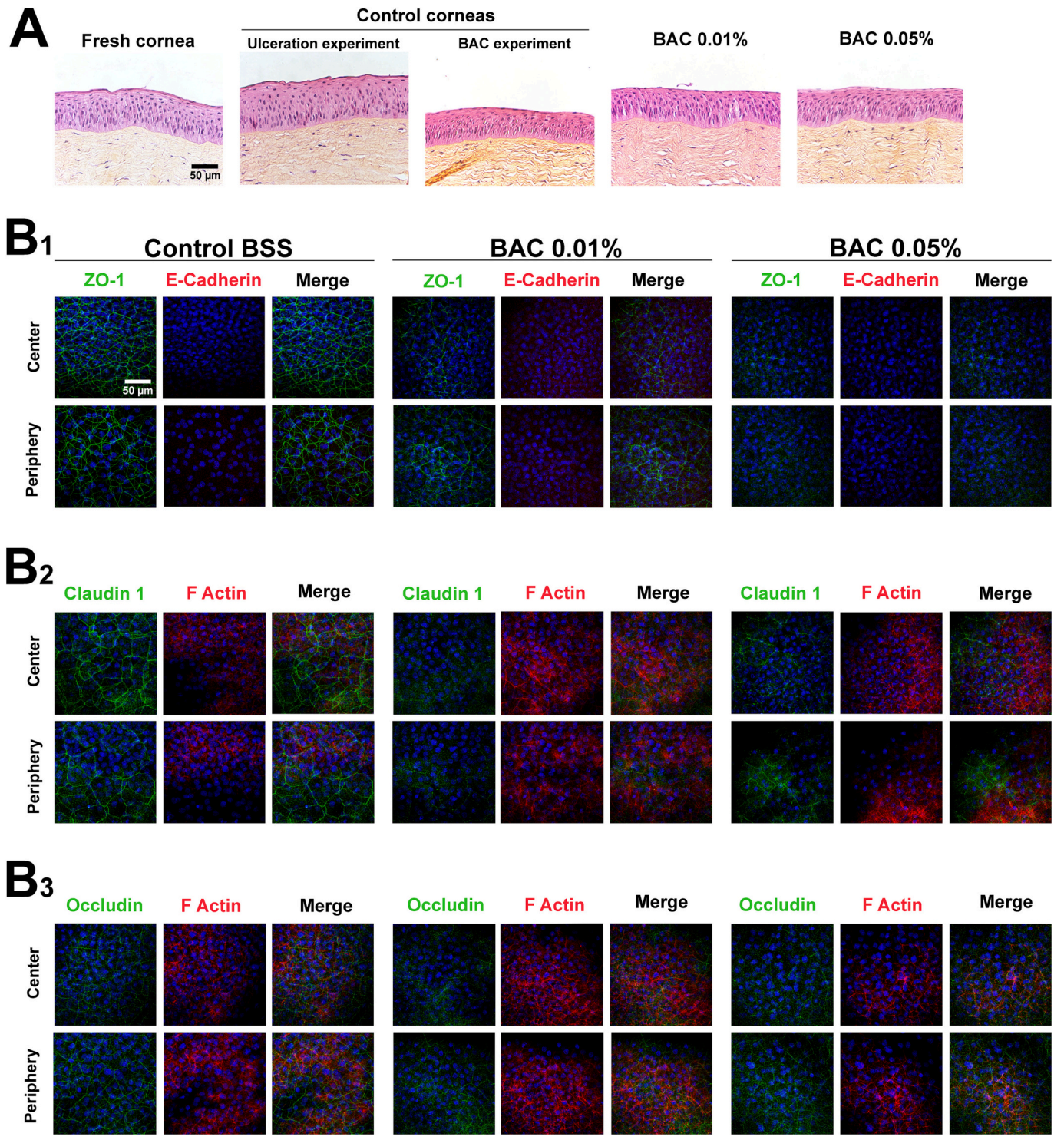

Fig. 4. Histology and immunohistology of porcine corneas. A/ Representative light microscope images of hematoxylin-eosin-saffron stained histological sections of porcine corneas from different experimental conditions (x40 magnification). B/ Representative immunostaining of ZO-1 (B1), claudin 1 (B2) and occludin (B3) performed on flat-mounted porcine corneas after BAC experiment for the 3 experimental groups (Control [BSS], BAC 0.01 and 0.05%) (x60 magnification). The studied marker was co-labeled with either E-cadherin (ZO-1) or filamentous actin by phalloidin dye (claudin 1 and occludin). Nuclei stained by DAPI were visible in blue. Images from both corneal center and periphery were displayed. (For interpretation of the references to colour in this figure legend, the reader is referred to the web version of this article.)

Klyce (Klyce, 1972). The study of trans-epithelial potential across corneal tissue showed three main regions of potential variation related to 3 regions of resistance: the apical membrane of squamous cells, the interface between wing and basal cells and finally to the basal membrane of basal cells. A simplified version of this model is widely used to describe the contribution of the transcellular and paracellular pathways across corneal epithelium (Nakamura et al., 2010; Uematsu et al., 2007). Interestingly, the impedance decrease triggered by BAC application was associated with a constant decrease of R1 alone, with no variation of the other parameters, whereas the removal of epithelium was associated

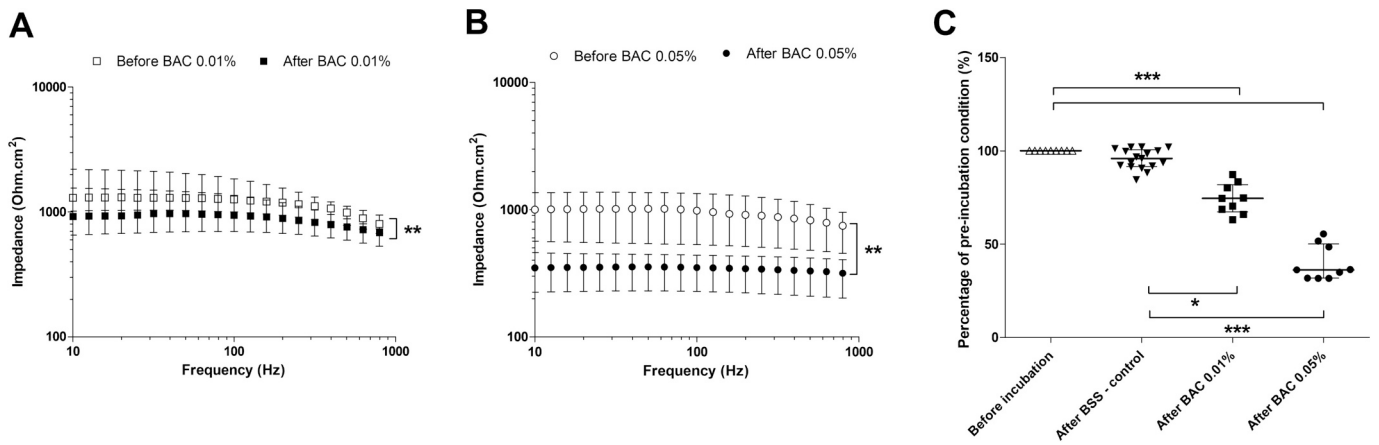

Fig. 5. Evolution of corneal impedance in response to an acute exposure to benzalkonium chloride (BAC) 0.01% (A) and 0.05% (B). Corneal impedance is expressed in Ω.cm2 (median with interquartile range) over the 10–1000 Hz range, before and after a 2-min incubation of the epithelial surface with BAC. **p < 0.001, Friedman test with Dunn's post-hoc analysis. C/ Impedance AUC values expressed as percentage of the baseline value (before incubation with BAC or BSS) for the tested (n = 9 corneas per BAC concentration) and the control corneas ($n = 17$). *$p < 0.01$ and ***$p < 0.0001$, Kruskal Wallis test with Dunn's post-hoc analysis.

with a drastic decrease in R1 and R3, and major C3 increase (Table S3). The decrease of R1 in response to BAC application support this R1 resistance to be associated with the paracellular pathway, controlled by intercellular tight junctions at the most superficial region of the epithelium, and described as one of major contributors of corneal epithelial barrier (Leong and Tong, 2015). On the other hand, the alteration of R1, R3 and C3 parameters in response to epithelial removal reflects the major contributions of these 3 parameters in the impedance signal measured and the global implication of both capacitive and resistive properties of corneal epithelium.

3.5. Corneal impedance in human corneas preserved in ASM

The evolution of corneal epithelial morphology was checked out by light macroscopy and OCT imaging during the 14-days storage in ASM (Fig. S3).

Impedance measured at D0 in human corneas with varying duration of OC differed among the studied corneas (Fig. 6). Corneal pair 1, that underwent the longest OC duration (7 weeks), presented the lowest impedance values at D0 (comparable to blank values) whereas impedance curves of corneal pair 2 and pair 3 were comparable (OC duration of 3 and 1 week respectively). Of note, impedance measured in the 2 corneas of a same pair was significantly different at D0 for pair 2 and pair 3 ($p < 0.05$, Friedman test with Dunn's post-hoc analysis). Fourteen days of storage in ASM resulted in a significant increase in corneal impedance in one cornea of each pair ($p < 0.05$, Friedman test with Dunn's post-hoc analysis), whereas the impedance increase in the contralateral cornea did not reach statistical significance. As for D0, the impedance measured at D14 in corneal pair 1 was significantly lower than impedance measured in the corneas of the two other pairs, except for the left cornea of pair 2. Indeed, this cornea was the only one to show unmodified impedance after the 14-days storage period.

Expression of tight junctions' proteins at D14 was explored by immunostaining on flat-mounted human corneas immediately after impedance measures. As both corneas of each pair were used in the experiment and could not be used as D0 control for immunostaining procedure, we used 2 corneas stored for 3 weeks in OC (as Pair 2) to explore tight junctions' proteins in corneas not stored in ASM (equivalent to D0 state).

The expression pattern of ZO-1, claudin 1 and occludin, localized at the most superficial layers, was comparable in the 2 OC corneas and was highly heterogenous and scarce (Fig. S4-A). ZO-1 labeling localized both at the cytoplasmic membrane and also in the cytoplasm of some cells. ZO-1 and claudin 1 labeling at the cytoplasmic membrane was highly discontinuous whereas occludin labelling was almost absent.

After 14-days storage in ASM, ZO-1 labeling resulted in a continuous linear pattern allowing the observation of large geometric cells typical of the most superficial corneal squamous cells (Fig. 7-A). Claudin 1

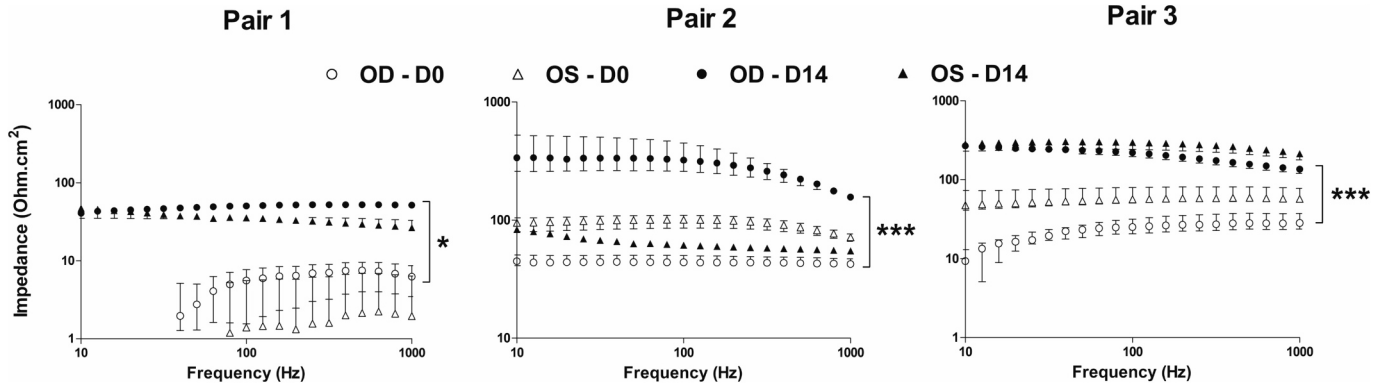

Fig. 6. Evolution of human corneal impedance in response to 14-days storage in Active Storage Machine (ASM). Corneal impedance is expressed in $\Omega.cm^2$ (median with interquartile range) over the 10–1000 Hz range. The impedance measured in each pair of corneas ($n = 3$) at D0 (corneas stored in organoculture conditions) and D14 (after 14-days in ASM) is represented separately. Impedance values under blank values were not represented (pair 1). Statistical results are represented for the comparison between D0 and D14 for each cornea. *p and ***p < 0.05, Friedman test with Dunn's post-hoc analysis. OD (*oculus dexter)*, right eye; OS (*oculus sinister)*, left eye.

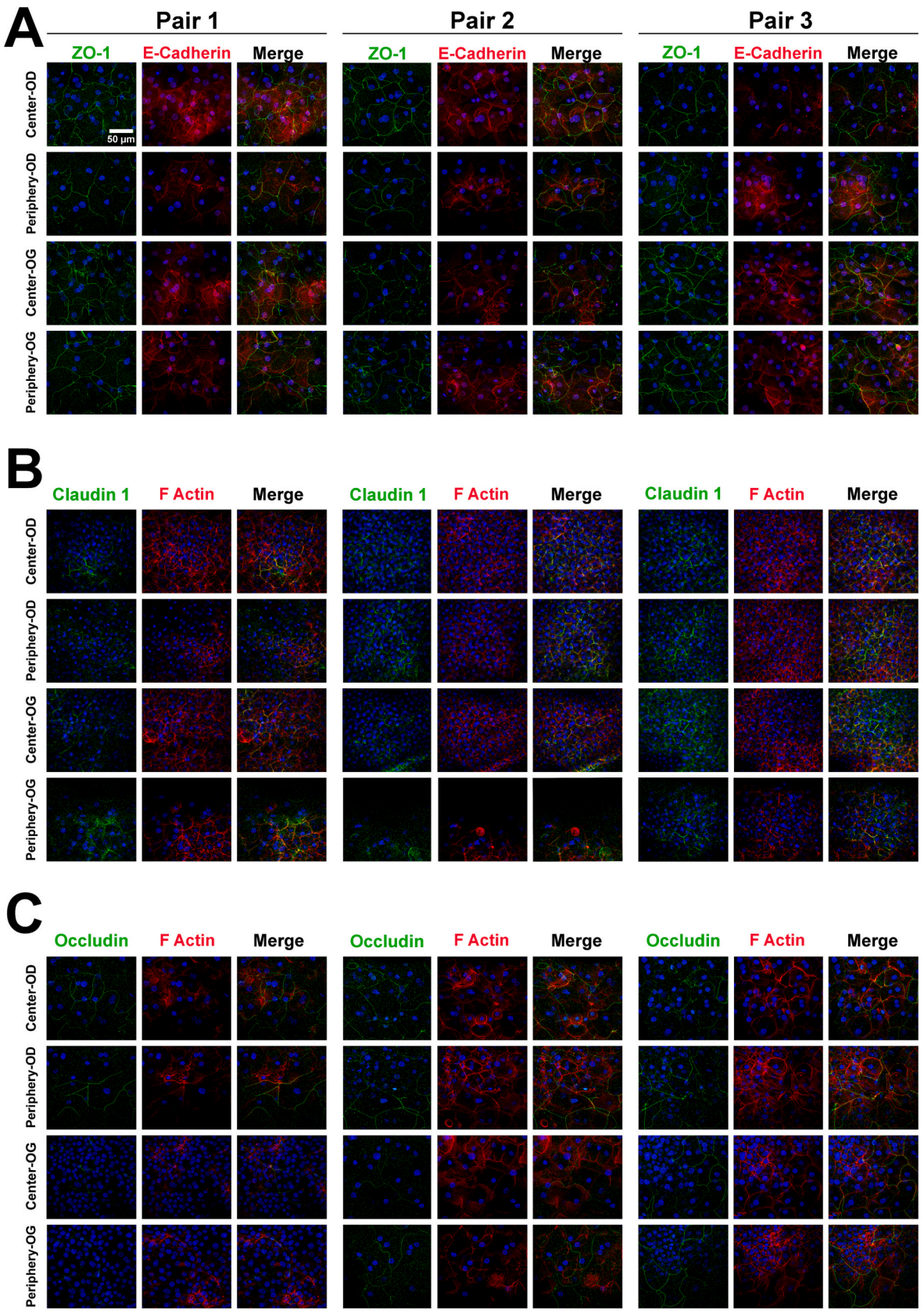

Fig. 7. Exploration of tight junction markers by immunohistology on flat-mounted human corneas. Representative immunostaining of ZO-1 (A), claudin 1 (B) and occludin (C) performed on flat-mounted human corneas from the three experimental pairs fixed immediately after D14 impedance measurement (x60 magnification). The studied marker is co-labeled with either E-cadherin (ZO-1) or filamentous actin by phalloidin dye (claudin 1 and occludin). Nuclei stained by DAPI are visible in blue. Images from both corneal center and periphery are displayed for the right (OD, *oculus dexter*) and the left cornea (OS, *oculus sinister*) for each pair. (For interpretation of the references to colour in this figure legend, the reader is referred to the web version of this article.)

labelling differs from ZO-1, with slightly less continuous and clear pattern highlighting the membrane of smaller cells, supporting a less superficial expression of the protein (Fig. 7-B). Occludin presented the more discontinuous and patchier labeling over the corneal surface (Fig. 7-C). When comparing the pair of corneas, ZO-1 labeling was similar among the corneas whereas pair 3 presented a more even labelling of claudin 1. Occludin labelling was also slightly less marked in OS of pair 1 and 2.

Taken together, these results highlight an evident improvement of tight junction's proteins expression that correlates with the increase in corneal impedance observed at D14, and support a higher degree of epithelial maturity. These observations are in accordance with our previous results of ASM development (Guindolet et al., 2021) and support the interest of corneal impedance technique to characterize the corneal epithelial barrier in a non-invasive way. In future experiment, exploration of the correlation between corneal impedance and tight junction proteins expression (by western blot) would allow defining more precisely the relationship between histological maturity and electrical properties of the cornea. A better understanding of this relationship is required to improve the interpretation of impedance values and to use it in the exploration and improvement of ASM storage conditions.

This would ultimately allow to fix a highly pertinent human corneal pharmacological model in ASM, but also to monitor the effect of pharmacological molecules on the human corneal tissue.

4. Conclusions

In this study, we have developed and validated a simple and cost-effective setup adapted to evaluate corneal electrical impedance in human samples stored in ASM. Validation step in fresh porcine corneas brings the observation of corneal impedance decrease in parallel to incremental physical and chemical damage of corneal epithelial barrier. When applied to human corneas stored in ASM, the set-up allowed us for the first time to highlight a significant increase in corneal impedance after 14 days of storage in ASM, that was correlated with the restoration of a multi-layer epithelium and an enhanced expression of tight-junctions markers, studied by histology and immunohistology. These first results support the use of this approach for non-invasive follow-up of corneal barrier integrity during corneal storage in ASM and help us in developing a well-characterized physiological model to explore trans-corneal drug penetration using human corneas.

Funding

This work was supported by Jean Monnet Medecine Faculty and Région Auvergne-Rhône-Alpes (Pack ambition recherche 2019 for BanCCo project, grant number 19 010225 01).

CRediT authorship contribution statement

Marielle Mentek: Writing – review & editing, Writing – original draft, Visualization, Supervision, Methodology, Investigation, Formal analysis, Conceptualization. **Benjamin Peyret:** Writing – original draft, Visualization, Investigation, Formal analysis, Data curation. **Siwar Zouari:** Investigation, Formal analysis. **Sébastien Urbaniak:** Visualization, Software, Methodology, Investigation, Data curation. **Jean-Marie Papillon:** Software, Resources, Data curation, Conceptualization. **Emmanuel Crouzet:** Resources, Methodology, Formal analysis. **Chantal Perrache:** Validation, Resources, Project administration, Investigation. **Sophie Hodin:** Validation, Resources, Formal analysis. **Xavier Delavenne:** Writing – review & editing, Supervision, Conceptualization. **Zhiguo He:** Writing – review & editing, Methodology. **Philippe Gain:** Writing – review & editing, Supervision, Project administration, Funding acquisition, Conceptualization. **Gilles Thuret:** Writing – review & editing, Supervision, Project administration, Funding acquisition, Conceptualization.

Declaration of competing interest

The authors declare the following financial interests/personal relationships which may be considered as potential competing interests:

Philippe Gain reports financial support was provided by Région Auvergne-Rhône-Alpes (France). Philippe Gain, Gilles Thuret has patent #EP2991479B1 issued to Francais du Sang Ets, Universite Jean Monnet Saint Etienne, Ecole Nationale dIngenieurs de Saint Etienne ENISE.

Data availability

All the data are shared in the manusript and supplementary data file

Acknowledgements

The authors acknowledge Dr. JM Dumollard and the team of pathology department of Saint-Etienne University Hospital Center for their support in tissue analysis, the slaughterhouse in Yssingeaux (Haute-Loire, France) for providing porcine eyeglobes, and Jean Monnet Faculty of Medicine and Région Auvergne-Rhône-Alpes for funding this work.

Appendix A. Supplementary data

Supplementary data to this article can be found online at https://doi.org/10.1016/j.ijpx.2024.100234.

References

Agarwal, P., Rupenthal, I.D., 2016. In vitro and ex vivo corneal penetration and absorption models. Drug Deliv. Transl. Res. 6, 634–647. https://doi.org/10.1007/s13346-015-0275-6.

Ban, Y., Dota, A., Cooper, L.J., Fullwood, N.J., Nakamura, T., Tsuzuki, M., Mochida, C., Kinoshita, S., 2003. Tight junction-related protein expression and distribution in human corneal epithelium. Exp. Eye Res. 76, 663–669. https://doi.org/10.1016/s0014-4835(03)00054-x.

Benson, K., Cramer, S., Galla, H.-J., 2013. Impedance-based cell monitoring: barrier properties and beyond. Fluids Barriers CNS 10, 5. https://doi.org/10.1186/2045-8118-10-5.

Biermann, H., Boden, K., Reim, M., 1991. Measuring electrical impedance in normal and pathologic corneas. Fortschr. Ophthalmol. 88, 17–20.

Chen, W., Li, Z., Hu, J., Zhang, Z., Chen, L., Chen, Y., Liu, Z., 2011. Corneal alternations induced by topical application of benzalkonium chloride in rabbit. PLoS One 6, e26103. https://doi.org/10.1371/journal.pone.0026103.

Chen, W., Hu, J., Zhang, Z., Chen, L., Xie, H., Dong, N., Chen, Y., Liu, Z., 2012. Localization and expression of zonula occludins-1 in the rabbit corneal epithelium following exposure to benzalkonium chloride. PLoS One 7, e40893. https://doi.org/10.1371/journal.pone.0040893.

Chetoni, P., Burgalassi, S., Monti, D., Saettone, M.F., 2003. Ocular toxicity of some corneal penetration enhancers evaluated by electrophysiology measurements on isolated rabbit corneas. Toxicol. in Vitro 17, 497–504. https://doi.org/10.1016/s0887-2333(03)00052-3.

Courrier, E., Maurin, C., Lambert, V., Renault, D., Bourlet, T., Pillet, S., Verhoeven, P.O., Forest, F., Perrache, C., He, Z., Garcin, T., Rousseau, A., Labetoulle, M., Gain, P., Thuret, G., 2020. Ex vivo model of herpes simplex virus type I dendritic and geographic keratitis using a corneal active storage machine. PLoS One 15, e0236183. https://doi.org/10.1371/journal.pone.0236183.

Donn, A., Maurice, D.M., Mills, N.L., 1959. Studies on the living cornea in vitro. I. Method and physiologic measurements. Arch. Ophthalmol. 62, 741–747. https://doi.org/10.1001/archopht.1959.04220050003001.

Fukuda, M., Sasaki, H., 2012. Quantitative evaluation of corneal epithelial injury caused by n-heptanol using a corneal resistance measuring device in vivo. Clin. Ophthalmol. 6, 585–593. https://doi.org/10.2147/OPTH.S30935.

Gabriel, C., 1995. The dielectric properties of biological materials. In: Klauenberg, B.J., Grandolfo, M., Erwin, D.N. (Eds.), Radiofrequency Radiation Standards: Biological Effects, Dosimetry, Epidemiology, and Public Health Policy, NATO ASI Series. Springer US, Boston, MA, pp. 187–196. https://doi.org/10.1007/978-1-4899-0945-9_20.

Gain, P., Jullienne, R., He, Z., Aldossary, M., Acquart, S., Cognasse, F., Thuret, G., 2016. Global survey of corneal transplantation and eye banking. JAMA Ophthalmol. 134, 167–173. https://doi.org/10.1001/jamaophthalmol.2015.4776.

Garcin, T., Gauthier, A.-S., Crouzet, E., He, Z., Herbepin, P., Perrache, C., Acquart, S., Cognasse, F., Forest, F., Thuret, G., Gain, P., 2019. Innovative corneal active storage machine for long-term eye banking. Am. J. Transplant. 19, 1641–1651. https://doi.org/10.1111/ajt.15238.

Garcin, T., Gauthier, A.-S., Crouzet, E., He, Z., Herbepin, P., Perrache, C., Acquart, S., Cognasse, F., Forest, F., Gain, P., Thuret, G., 2020. Three-month storage of human corneas in an active storage machine. Transplantation 104, 1159–1165. https://doi.org/10.1097/TP.0000000000003109.

Guimera, A., Gabriel, G., Plata-Cordero, M., Montero, L., Maldonado, M.J., Villa, R., 2012. A non-invasive method for an in vivo assessment of corneal epithelium permeability through tetrapolar impedance measurements. Biosens. Bioelectron. 31, 55–61. https://doi.org/10.1016/j.bios.2011.09.039.

Guimerà, A., Illa, X., Traver, E., Plata-Cordero, M., Yeste, J., Herrero, C., Lagunas, C., Maldonado, M.J., Villa, R., 2013. Flexible probe for in vivo quantification of corneal epithelium permeability through non-invasive tetrapolar impedance measurements. Biomed. Microdevices 15, 849–858. https://doi.org/10.1007/s10544-013-9772-x.

Guindolet, D., Crouzet, E., He, Z., Herbepin, P., Jumelle, C., Perrache, C., Dumollard, J. M., Forest, F., Peoc'h, M., Gain, P., Gabison, E., Thuret, G., 2017. Storage of porcine cornea in an innovative bioreactor. Invest. Ophthalmol. Vis. Sci. 58, 5907–5917. https://doi.org/10.1167/iovs.17-22218.

Guindolet, D., Crouzet, E., He, Z., Herbepin, P., Perrache, C., Garcin, T., Gauthier, A.-S., Forest, F., Peoc'h, M., Gain, P., Gabison, E., Thuret, G., 2021. Epithelial regeneration in human corneas preserved in an active storage machine. Transl. Vis. Sci. Technol. 10, 31. https://doi.org/10.1167/tvst.10.2.31.

Juretić, M., Cetina-Čižmek, B., Filipović-Grčić, J., Hafner, A., Lovrić, J., Pepić, I., 2018. Biopharmaceutical evaluation of surface active ophthalmic excipients using in vitro and ex vivo corneal models. Eur. J. Pharm. Sci. 120, 133–141. https://doi.org/10.1016/j.ejps.2018.04.032.

Jürgens, I., Rosell, J., Riu, P.J., 1996. Electrical impedance tomography of the eye: in vitro measurements of the cornea and the lens. Physiol. Meas. 17 (Suppl 4A), A187–A195. https://doi.org/10.1088/0967-3334/17/4a/023.

Kaluzhny, Y., Klausner, M., 2021. In vitro reconstructed 3D corneal tissue models for ocular toxicology and ophthalmic drug development. In Vitro Cell. Dev. Biol. Anim. 57, 207–237. https://doi.org/10.1007/s11626-020-00533-7.

Klyce, S.D., 1972. Electrical profiles in the corneal epithelium. J. Physiol. 226, 407–429. https://doi.org/10.1113/jphysiol.1972.sp009991.

Kusano, M., Uematsu, M., Kumagami, T., Sasaki, H., Kitaoka, T., 2010. Evaluation of acute corneal barrier change induced by topically applied preservatives using corneal transepithelial electric resistance in vivo. Cornea 29, 80–85. https://doi.org/10.1097/ICO.0b013e3181a3c3e6.

Leong, Y.-Y., Tong, L., 2015. Barrier function in the ocular surface: from conventional paradigms to new opportunities. Ocul. Surf. 13, 103–109. https://doi.org/10.1016/j.jtos.2014.10.003.

Ma, L., Kuang, K., Smith, R.W., Rittenband, D., Iserovich, P., Diecke, F.P.J., Fischbarg, J., 2007. Modulation of tight junction properties relevant to fluid transport across rabbit corneal endothelium. Exp. Eye Res. 84, 790–798. https://doi.org/10.1016/j.exer.2006.12.018.

Macdonald, J.R., Johnson, W.B., Raistrick, I.D., Franceschetti, D.R., Wagner, N., Mckubre, M., Macdonald, D., Sayers, B., Bonanos, N., Steele, B.C.H., Butler, E.P., Worell, W.L., Strømme, M., Malmgren, S., Sundaram, S., Engelhardt, G.R., Barsukov, Y., Pell, W.G., Roland, C.M., Eisenberg, R., 2018. Impedance Spectroscopy: Theory, Experiment, and Applications, Third edition.

Maulvi, F.A., Shetty, K.H., Desai, D.T., Shah, D.O., Willcox, M.D.P., 2021. Recent advances in ophthalmic preparations: Ocular barriers, dosage forms and routes of administration. Int. J. Pharmaceut. 608, 121105 https://doi.org/10.1016/j.ijpharm.2021.121105.

Nakamura, T., Yamada, M., Teshima, M., Nakashima, M., To, H., Ichikawa, N., Sasaki, H., 2007. Electrophysiological characterization of tight junctional pathway of rabbit cornea treated with ophthalmic ingredients. Biol. Pharm. Bull. 30, 2360–2364. https://doi.org/10.1248/bpb.30.2360.

Nakamura, T., Teshima, M., Kitahara, T., Sasaki, H., Uematsu, M., Kitaoka, T., Nakashima, M., Nishida, K., Nakamura, J., Higuchi, S., 2010. Sensitive and real-time method for evaluating corneal barrier considering tear flow. Biol. Pharm. Bull. 33, 107–110. https://doi.org/10.1248/bpb.33.107.

Obeid, H., Khettab, H., Marais, L., Hallab, M., Laurent, S., Boutouyrie, P., 2017. Evaluation of arterial stiffness by finger-toe pulse wave velocity: optimization of signal processing and clinical validation. J. Hypertens. 35, 1618–1625. https://doi.org/10.1097/HJH.0000000000001371.

Potts, A.M., Modrell, R.W., 1957. The transcorneal potential*. Am. J. Ophthalmol. 44, 284–290. https://doi.org/10.1016/0002-9394(57)93123-9.

Prausnitz, M.R., Noonan, J.S., 1998. Permeability of cornea, sclera, and conjunctiva: a literature analysis for drug delivery to the eye. J. Pharm. Sci. 87, 1479–1488. https://doi.org/10.1021/js9802594.

Ray, S., Kassan, A., Busija, A.R., Rangamani, P., Patel, H.H., 2016. The plasma membrane as a capacitor for energy and metabolism. Am. J. Phys. Cell Physiol. 310, C181–C192. https://doi.org/10.1152/ajpcell.00087.2015.

Rojanasakul, Y., Robinson, J.R., 1990. Electrophysiological and ultrastructural characterization of the cornea during in vitro perfusion. Int. J. Pharmaceut. 63, 1–16. https://doi.org/10.1016/0378-5173(90)90094-K.

Rojanasakul, Y., Liaw, J., Robinson, J.R., 1990. Mechanisms of action of some penetration enhancers in the cornea: laser scanning confocal microscopic and electrophysiology studies. Int. J. Pharmaceut. 66, 131–142. https://doi.org/10.1016/0378-5173(90)90392-H.

Schwan, H.P., 1957. Electrical properties of tissue and cell suspensions. Adv. Biol. Med. Phys. 5, 147–209. https://doi.org/10.1016/b978-1-4832-3111-2.50008-0.

Srinivasan, B., Kolli, A.R., Esch, M.B., Abaci, H.E., Shuler, M.L., Hickman, J.J., 2015. TEER measurement techniques for in vitro barrier model systems. J. Lab. Autom. 20, 107–126. https://doi.org/10.1177/2211068214561025.

Uematsu, M., Kumagami, T., Kusano, M., Yamada, K., Mishima, K., Fujimura, K., Sasaki, H., Kitaoka, T., 2007. Acute corneal epithelial change after instillation of benzalkonium chloride evaluated using a newly developed in vivo corneal transepithelial electric resistance measurement method. Ophthalmic Res. 39, 308–314. https://doi.org/10.1159/000109986.

Uematsu, M., Mohamed, Y.H., Onizuka, N., Ueki, R., Inoue, D., Fujikawa, A., Kitaoka, T., 2015. A novel in vivo corneal trans-epithelial electrical resistance measurement device. J. Pharmacol. Toxicol. Methods 76, 65–71. https://doi.org/10.1016/j.vascn.2015.08.153.

Uematsu, M., Mohamed, Y.H., Onizuka, N., Ueki, R., Inoue, D., Fujikawa, A., Sasaki, H., Kitaoka, T., 2016. Less invasive corneal transepithelial electrical resistance measurement method. Ocul. Surf. 14, 37–42. https://doi.org/10.1016/j.jtos.2015.07.004.

Vaede, D., Baudouin, C., Warnet, J.-M., Brignole-Baudouin, F., 2010. Preservatives in eye drops: toward awareness of their toxicity. J. Fr. Ophtalmol. 33, 505–524. https://doi.org/10.1016/j.jfo.2010.06.018.

Vandenhaute, E., 2011. Établissement et caractérisation de nouveaux modèlesin vitro de barrière hémato-encéphalique : de la recherche fondamentale à la recherche appliquée (phdthesis). Université d'Artois.

Wu, S., Ketcham, S.A., Corredor, C.C., Both, D., Drennen, J.K., Anderson, C.A., 2022. Rapid at-line early cell death quantification using capacitance spectroscopy. Biotechnol. Bioeng. 119, 857–867. https://doi.org/10.1002/bit.28011.

Zhang, G., Zhu, R., 2010. Effect of parasitic capacitance on impedance measurement and model extraction. Electroanalysis 22, 351–358. https://doi.org/10.1002/elan.200900324.